Fast flow microfluidics and single-molecule fluorescence for the rapid characterization of alpha-synuclein oligomers

Authors: *Mathew H. Horrocks[1†], Laura Tosatto[1,2†], Alexander J. Dear[1], Gonzalo A. Garcia[1], Marija Iljina[1], Nunilo Cremades[1], Mauro Dalla Serra[2], Tuomas P. J. Knowles[1], Christopher M. Dobson[1], David Klenerman.[1]**

Author Addresses: [1]Department of Chemistry, University of Cambridge, Lensfield Road, Cambridge CB2 1EW, UK.

[2]Istituto di Biofisica, CNR, U.O. Trento, Italy

*Correspondence to: dk10012@cam.ac.uk.

[†]These authors contributed equally to this work.

Abstract:

Alpha-synuclein oligomers can be toxic to cells and may be responsible for cell death in Parkinson's disease. Their typically low abundance and highly heterogeneous nature, however, make such species challenging to study using traditional biochemical techniques. By combining fast-flow microfluidics with single-molecule fluorescence, we

are able to rapidly follow the process by which oligomers of αS are formed, and to characterize the species themselves. We have used the technique to show that populations of oligomers with different FRET efficiencies have varying stabilities when diluted into low ionic strength solutions. Interestingly, we have found that oligomers formed early in the aggregation pathway have electrostatic repulsions that are shielded in the high ionic strength buffer, and therefore dissociate when diluted into lower ionic strength solutions. This property can be used to isolate different structural groups of αS oligomers and can help to rationalize some aspects of αS amyloid fibril formation.

Introduction

Parkinson's disease (PD) is the second most common neurodegenerative disease after Alzheimer's disease[1], affecting more than 1% of the world's population of those aged over 65 years[2]. Clinically, the disorder is characterized by a loss of control of movement, and the onset of resting tremors, muscle rigidity and bradykinesia. Additionally, there are non-motor characteristics, such as cognitive impairment, depression, olfactory deficits, psychosis, and sleep disturbance during the progression of the disease[3]. Neuropathologically, PD is characterized by the progressive loss of dopaminergic neurons within the *substantia nigra pars compacta* of the midbrain. One of the major pathological hallmarks of PD is the presence of intra-neuronal proteinaceous cytoplasmic inclusions, referred to as Lewy Bodies (LBs). The finding that amyloid fibrils of the protein alpha-synuclein (αS) are a major component of LBs suggests that it is involved in the etiology of the disease[4]. LBs are also found in other neurodegenerative disorders such as Dementia with LBs, the LB variant of AD[5] and Down's Syndrome[6]. Duplication[7] and

triplication[8] of the chromosomal region surrounding the gene coding for αS, and a number of point mutations[8–13] lead to dominantly inherited PD, providing further evidence for the link between the protein and the diseases.

The finding that purified recombinant αS forms fibrils resembling those found in LBs[14] has led to speculation that aggregation plays a key role in the disease. When αS aggregates *in vitro,* small soluble oligomers, which have been shown to be cytotoxic, are generated[15–17], and such species can, in some cases, progress directly into fibrillar structures. Despite the evidence of their importance to the disease, the usually low abundance and highly heterogeneous nature of the oligomeric species formed during the aggregation reaction make them difficult to study using traditional biochemical techniques. We have previously used single-molecule fluorescence techniques to characterize the aggregation and behavior of amyloid oligomers of the SH3 domain of PI3 kinase[18], the amyloid-beta peptide[19,20] and αS[16]. For the latter, we used single-molecule Förster Resonance Energy Transfer (FRET) to show that αS initially forms amorphous oligomers having a low FRET efficiency, which consequently undergo a structural rearrangement to form proteinase-K resistant, cytotoxic oligomers, having a higher FRET efficiency[16].

The oligomers of αS generated during fibril formation typically only make up a small fraction of the total protein concentration, and so single-molecule techniques are needed to detect their presence and characterize their structures. The picomolar concentrations required for single-molecule detection, however, mean that a significant time is needed to collect enough data to make useful conclusions. Through incorporating fast-flow microfluidics (*Figure 1*) to rapidly pass the low concentration solutions through the

confocal volume (at a velocity of 2 cm/s), we have now reduced the data acquisition time from 3 hours, to just over 5 minutes per time-point, thereby allowing us to increase drastically the time-resolution of our technique, and also to run several aggregations on one instrument simultaneously. In this paper, we illustrate the power of this technique by studying in more detail the aggregation of αS.

The conformation of monomeric αS is affected by factors such as pH[21] and ionic strength[22], and we speculated that certain types of oligomers may be electrostatically destabilized due to inter monomer electrostatic repulsion because of the high net charge of the C-terminal region. To test this hypothesis, we used the increased data-acquisition rate of this technique to study the effect of diluting the time-points from the aggregation into high and low ionic strength buffers. We found that the amorphous type oligomers, which are less cytotoxic, and more susceptible to proteinase-K digestion, dissociate at low ionic strengths, whereas the higher FRET species are stable to such a change in conditions.

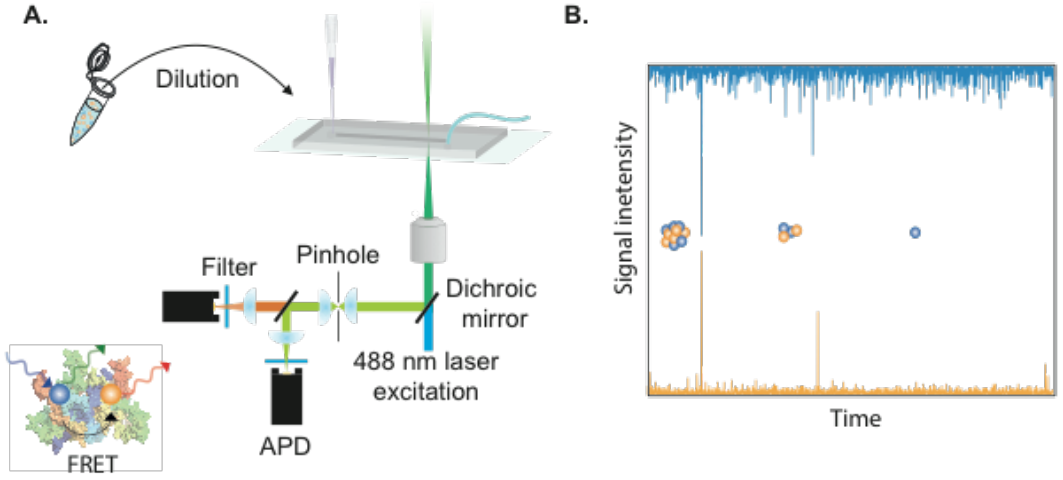

Figure 1. A. Instrumental setup. The microfluidic device is mounted onto a confocal microscope in which 488 nm radiation is focused down to a diffraction-limited spot

within the 100 μm wide channel. Fluorescence from Alexa Fluor 488 (AF488) and Alexa Fluor 594 (AF594) (excited indirectly via FRET) can then be collected, and separated onto two separate Avalanche photodiode detectors (APDs). B. Example intensity traces. Bursts of intensity arise when fluorescently labeled αS transits the confocal volume. Oligomeric species have a burst in both the donor (blue trace) and acceptor (orange trace) channel, allowing them to be separated from the majority of monomeric protein (donor bursts only).

RESULTS AND DISCUSSION

Microfluidic device design

In order to determine whether an increase in the data acquisition rate for αS aggregation samples could be achieved using fast-flow, a simple microfluidic device was designed and made from PDMS. The device consists of a single channel, 100 μm in width, 25 μm in height and 1 cm in length. The width and height were selected to prevent larger fibrils blocking the device, and this is demonstrated by the constant monomer and oligomer detection rate over the duration of the measurement, even at later time-points when fibrils are present (*Figure 2*B and C.). The aggregation samples were diluted before being loaded into a low-binding gel-loading tip, which was inserted into the entry port of the device (*Figure 2*A.). Tubing connected to a syringe within a syringe pump was attached to the exit port, allowing for accurate control of the flow-velocity by application of a negative pressure. By withdrawing sample in this way, rather than infusing sample directly from a syringe, the dead volume was minimal, and the exposure of the samples to hydrophobic surfaces, such as the inside of plastic tubing, was minimized.

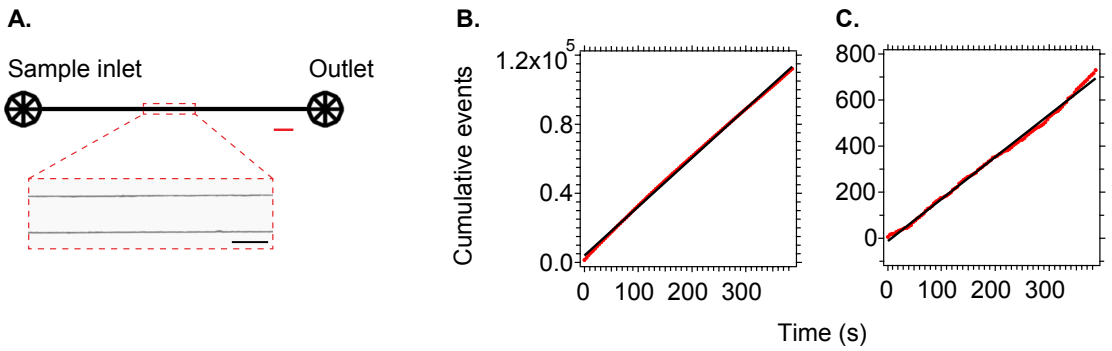

Figure 2. A. Device design. The microfluidic chip consists of a single-channel, 100 μm in *width, and 25 μm in height, red scale bar is 500 μm in length. A gel-loading tip containing the analyst is added to the sample inlet, and the outlet is attached to a syringe within a syringe pump to pull sample through the device. Zoom: Brightfield image of the microfluidic device channel (scale bar is 100 μm in length). B. and C. Cumulative frequency histogram of monomeric and oligomeric events, respectively, over a 400s measurement of 280 pM aggregated αS. The histograms are fitted to a straight line yielding* $R^2 = 0.999$ *and* $R^2 = 0.998$ *for monomeric, and oligomeric events, respectively. This shows that the event detection rate remains constant over the measurement time.*

Increase in data acquisition rate with fast flow microfluidics

Many steps in protein aggregation reactions are likely to take place on time-scales that are shorter than the 3 h time points used in our previous study on the oligomers formed during the aggregation of αS[16]. We sought to increase the time resolution by using fast flow microfluidics. It has previously been shown that it is possible to increase the rate of data acquisition in single-molecule confocal experiments by flowing the molecules through the probe volume at high speeds (see *Figure 1*)[23]. There is, however, an upper limit to the velocity at which molecules can flow through the confocal volume whilst still enabling the collection of meaningful data. At higher speeds, there is an increase in the rate at which fluorescent species transit the probe volume; in parallel, there is, however, a decrease in the number of excitation-emission cycles of the fluorophores, reducing event

brightness. Thus, there is an optimum velocity at which the event rate is high, but the brightness of the fluorescent bursts is not sufficiently low to make them undetectable. With two-color excitation, the rate at which it is possible to flow and still get meaningful data is higher than for the FRET experiments in which only one color is directly excited. For the work presented here, only the donor dyes are directly excited, and the presence of signal in the acceptor channel due to FRET is used to identify the oligomers in the presence of an excess of monomers. The oligomers, however, typically have more than one donor fluorophore present, and so it is possible to flow at higher velocities than those used for detecting species with only one directly excited donor dye.

To determine the optimum flow velocity for our experiment, an aliquot of αS solution was removed after incubation under aggregation conditions for 24 hours and diluted to 300 pM, before being flowed through a simple one-channel device mounted on the single-molecule confocal instrument at a range of velocities. With increasing flow velocity, it was necessary to increase the laser intensity, as under these conditions, the molecules spend less time in the confocal volume. The optimum intensities were determined previously[23] by selecting those laser powers that gave the highest brightness at each velocity, up to the maximum power achievable on our instrumental set-up. The brightness of the bursts is also dependent on the flow velocity, and so it was necessary to vary the thresholds (see Supporting Information for details of thresholding and data analysis) in the donor and acceptor channels for each flow velocity. To achieve this in an unbiased way, we have previously[23] shown that the thresholds at each flow velocity can be selected to give the maximum fraction of coincident fluorescent bursts in both channels using a dual labeled DNA duplex as an example[24]. The flow velocities, time

bin-widths, and automatically selected thresholds are presented in SI Table 1. *Figure 3* shows the effect of varying flow speed on the measured monomer brightness (*A*), and the donor channel burst-rate (*B*). Even with the increase in laser power that can be used at higher flow velocities, the monomer brightness decreases due to the molecules spending less time in the probe volume, and therefore completing fewer excitation-emission cycles. However, with increasing flow velocity, the donor burst-rate initially increases, reaching a maximum of 530 ± 115 burst s^{-1} at a rate of 5 cm/s. At higher velocities, there is a decrease in the number of monomers detected, as the dye molecules are unable to emit enough photons to be detected above the applied thresholds.

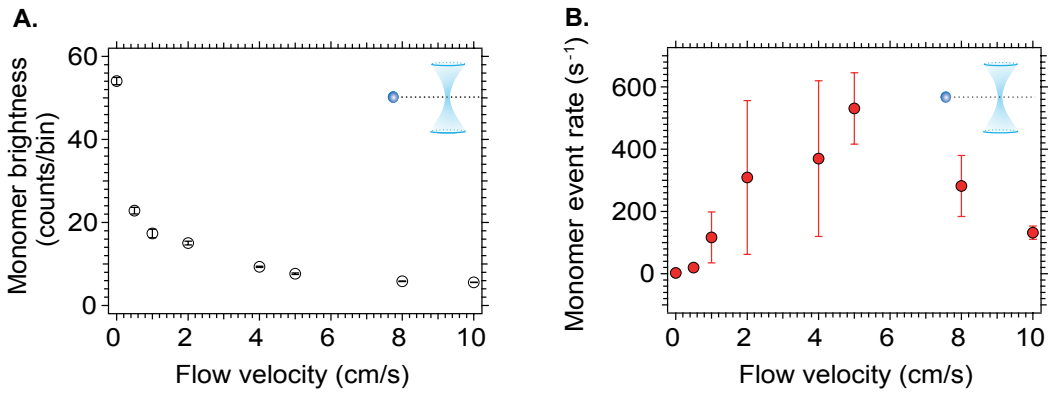

Figure 3. The effect of flow velocity on A. the measured mean monomer brightness, and B. the monomer burst rate (mean ± S.D., n = 3) when 280 pM of αS was passed through the microfluidic channel at varying flow velocities. With increasing flow velocity, the intensity of the bursts decreases due to fewer excitation-relaxation cycles in the shortened residence time in the probe volume. By contrast, the donor burst-rate initially increases, due to a faster encounter rate with the probe volume, but then decreases as a larger proportion of the molecules become insufficiently bright to detect.

As the oligomers are likely to contain more than one donor-labeled molecule, they are brighter than the monomer alone, and have a greater probability of emitting sufficient photons to be detected above the threshold level at higher flow velocities. *Figure 4A* shows the number of oligomers detected as a function of the mean flow velocity. As with the rate of monomer detection, there is an initial increase in the number of events detected as the flow velocity increases, before a slight decrease at higher velocities.

The association quotient, Q (defined in the Supporting Information), indicates the fraction of molecules that simultaneously exhibit bursts of fluorescence above the applied thresholds in both detection channels. *Figure 4B* shows how Q varies as a function of flow velocity for the oligomeric sample solution. Increasing the mean flow velocity from 0 to 0.5 cm s^{-1} leads to a slight increase in Q, as observed previously for dual-labeled DNA duplexes[23]. At higher velocities, there is a decrease in the Q value, due to the reduction in the brightness of the fluorophores, which are unable to complete sufficient excitation-emission cycles within the probe volume. In performing experiments under fast-flow, it is desirable that the flow velocity is high enough that many events are detected, but not so high that the number of photons detected limits the quality of the data. To take both of these factors into account in selecting the optimum flow velocity, the product of the event rate and Q against the varying flow speed was determined, and is plotted in *Figure 4C*. There is an increase in the product up to 2 cm/s, followed by a plateau at higher velocities indicating that a mean flow velocity of 2 cm/s is ideal for performing measurements of the oligomeric species under investigation here, since the event rate is increased (events are detected ~150 times more frequently than under static conditions), whilst the Q value is still reasonably high.

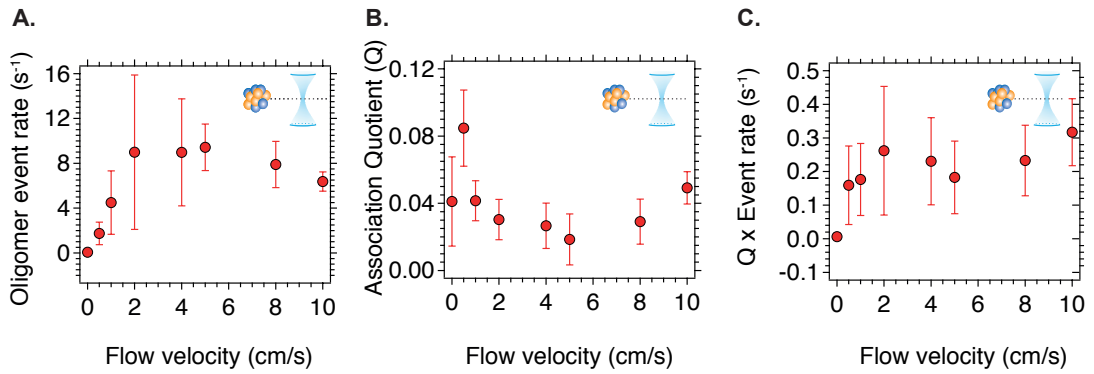

Figure 4 A. The effect of increasing flow velocity on the oligomer event rate when a 280pM sample of aggregated αS (starting monomer concentration) was passed through the microfluidic channel at varying flow velocities. With increasing flow rate, the event rate increases, making a plateau level after 2 cm/s, before decreasing slightly (mean ± S.D., n = 3). B. The association quotient as a function of flow velocity (mean ± S.D., n = 3). There is a slight increase in the association quotient in changing the flow velocity from 0 to 0.5 cm/s; however, it decreases at higher velocities due to the fluorophores being less bright, and therefore less easily detectable. At higher velocities still (> 5 cm/s), the association constant slightly increases; however, this is due to the significant decrease in the monomer event rate (Figure 1B). C. The product of the association quotient and event rate increases from 0 to 2 cm/s before plateauing (mean ± S.D., n = 3).

A further advantage of using microfluidic delivery to the confocal volume is that the flow velocity of the individual species is independent of their diffusivity/size, as the molecules are under laminar flow. In stationary measurements, relying on diffusion only, larger species are able to occupy the probe volume for a prolonged period of time, which

can lead to multiple counting of events. In addition, the path taken through the confocal volume is more constant under flow (i.e. the molecules flow in one-dimension, rather than traveling through via Brownian motion), meaning that the transit time remains constant, and any intensity changes due to varying residence time are removed. Also, since the flow is constant regardless of the species size, then species that are larger than the confocal volume diameter, such as fibrils, will occupy a greater number of time-bins than smaller species such as oligomers, as it takes a longer period of time for them to transit fully the confocal volume. This effect allows for fibrillar species to be separated from the smaller oligomeric events, which do not occupy multiple bins (see Supporting Information).

Following the kinetics of an *in vitro* aggregation of αS

To determine the ability of the enhanced methodology to follow the *in vitro* formation of αS oligomers, solutions of αS were incubated under conditions favoring aggregation, and aliquots were taken and analysed at regular time intervals using single-molecule fluorescence. As monomers become incorporated into oligomers and fibrils, their numbers decrease, and this effect can be observed in *Figure 4*, which shows the number of donor fluorescent bursts detected above the applied threshold within the 400 s measurement time for the 50 hour time-course of the aggregation reaction.

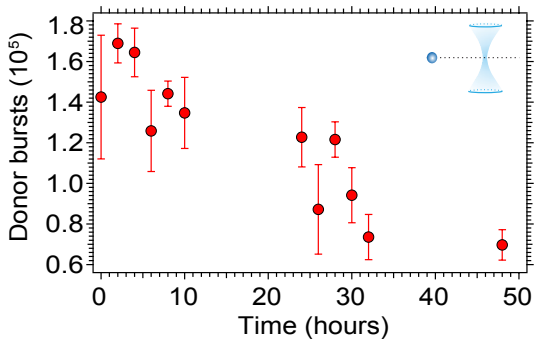

Figure 5. The change in the number of donor bursts measured over time during the aggregation of αS in 150 mM tris buffer with 100 mM NaCl (mean ± S.D., n = 3). The donor burst rate decreases as monomers are incorporated into oligomers and fibrils, because their concentration in solution is lower.

For each event detected, the FRET efficiency and approximate size of the oligomer giving rise to it can be determined (see Supporting Information for details), and then binned into histograms (*Figure 6A*). As time progresses, the range of the sizes increases; after six hours of incubation, there are few events attributable to an oligomer containing more than 10 monomer units, whereas after 48 hours of incubation, a significant number of events have larger sizes of up to 50 monomer units. This is expected as the oligomers grow in size through monomer addition. It is also evident that there is a transition from species with a low FRET efficiency to those with a high FRET efficiency as the aggregation progresses. After six hours of incubation, *95.9% ± 6.2% (mean ± S.D., n = 3) of the 3-150mers are within the lower FRET efficiency population, whereas at 48 hours, only 37.8% ± 4.2% (mean ± S.D., n=3) of them are within the lower FRET population.*

By generating FRET efficiency histograms from events corresponding to dimers, and species greater in size than trimers, it is possible to observe a change in the FRET efficiency more easily (*Figure 6B*). For the smaller apparently dimeric oligomers, only one FRET population is observed, although this could be a mixture of the two

populations observed for larger species (it also has a FRET efficiency in between those of the two populations of larger species), but since the events must have a greater number of photons than the applied thresholds in both the donor and acceptor channel, events with either very high or low FRET efficiencies and few emitted photons may not be detected, and this may prevent the two peaks from being resolved for the smaller sized oligomers. For the larger oligomers, two peaks can be clearly resolved and fitted to Gaussian distributions. After integrating the fitted FRET histograms, the changes in the number of oligomers within each population can be plotted (*Figure 6C*). All three populations show an increase in the number of oligomers over time; for the low FRET form of the larger oligomers (corresponding to the "type A" oligomers identified previously[16]), the increase appears to occur rapidly after 2 hours of incubation, and continues at a high rate during the first 10 hours. For the higher FRET larger species (corresponding to the "type B" oligomers), the increase does not occur until after 8 hours of incubation, and then continues at a steady rate for the rest of the time-period. This delay in their presence can be attributed to the fact that they are formed from the conversion of type A oligomers. The apparent dimers show a gradual increase throughout the time-course, as this population is formed from a mixture of the low and high FRET species that cannot be separated due to low photon counts.

In our previous study[16], the single-molecule data were fit to a nucleation growth model with a conformational conversion step, and we have used the same kinetic analysis here to analyze the analogous data. The model assumes that primary nucleation results in the creation of oligomers of type A from monomeric protein molecules, and that type A oligomers can grow through monomer addition, or can convert into type B oligomers,

resulting in several parallel pathways for the formation of type B oligomers of a given size (details of the early-time analytical and exact numerical solutions of the model are presented in the Supporting Information). Only the first six time-points here are fit with this model (*Figure 6D*.), since at later times, additional events, such as the formation of large fibrillar species, the contribution of the reverse processes involving conversion of type-B oligomers into type-A oligomers, and the dissociation of type-A oligomers, become significant and result in under-fitting of the data.

This method of fitting generates two well-defined microscopic parameters; the primary nucleation rate constant for oligomers of type A was found to be 1.05×10^{-7} s^{-1}, and the conversion rate constant from type A to type B oligomers as 2.02×10^{-5} s^{-1}. These values are similar to those determined previously[16], suggesting that the information obtained using single-molecule fluorescence and fast-flow microfluidics is fully consistent with the data taken without flow.

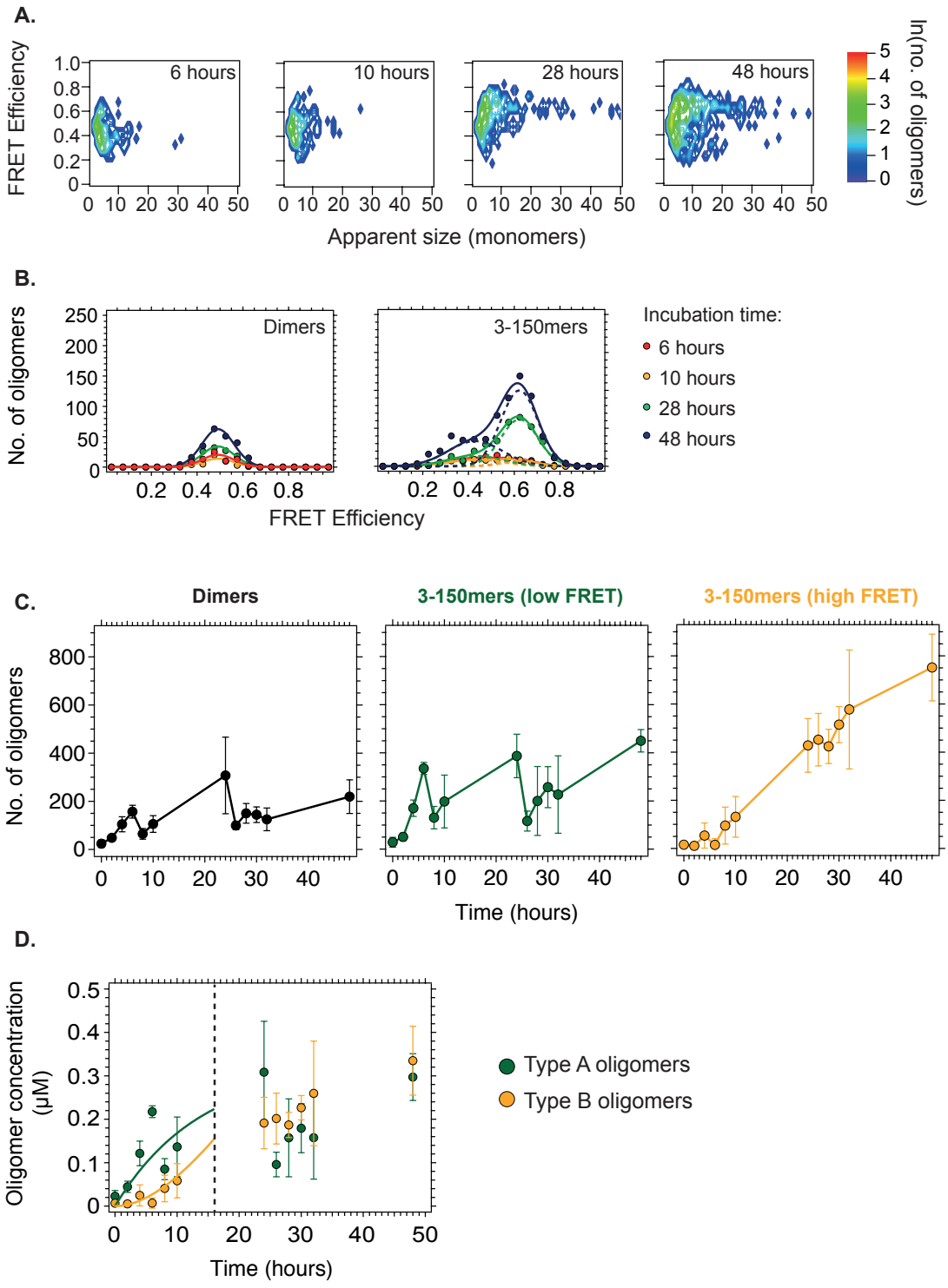
A.
FRET Efficiency
6 hours
10 hours
28 hours
48 hours
Apparent size (monomers)
ln(no. of oligomers)
B.
No. of oligomers
Dimers
3-150mers
FRET Efficiency
Incubation time:
6 hours
10 hours
28 hours
48 hours
C.
Dimers
3-150mers (low FRET)
3-150mers (high FRET)
No. of oligomers
Time (hours)
D.
Oligomer concentration (μM)
Time (hours)
Type A oligomers
Type B oligomers

Figure 6. A. 2D contour plots of size and FRET efficiency of various times from solutions of aggregating αS. The size and FRET efficiency both increase over time. B. FRET efficiency histograms for various time-points taken during the aggregation of αS. The oligomers are separated into two different size groupings for which the populations were identified. C. Kinetic traces for the three different populations of αS aggregates (mean ± S.D., n = 3). There is an increase in the number of oligomers over time; however, the major increase for the type A oligomers occurs in the first 24 hours, whereas for the type B species, the increase is in the second 24 hours. D. Results of the global fitting of the kinetics of formation of the type A and type B oligomers (solid green and yellow lines, respectively). The fitting is performed on the first six data-points (up to 10 hours), before fibrils can be identified by the presence of a pellet after centrifugation at 15,000 r.p.m. for 15 minutes.

Effect of varying ionic strength on the stability of oligomers:

In order to probe the nature of the interactions within the oligomeric species, we studied the effect of ionic strength on their stability. We examined two different samples, one formed after 14 hours of incubation in which there are mainly type A oligomers and the other after 38 hours in which there are mainly the type B oligomers. These samples were diluted into a solution of 5 mM tris buffer at pH 7.4 containing varying concentrations of NaCl to change the ionic strength. The FRET efficiency histograms are shown in SI Fig. 3 and 4, and *Figure 7* shows the number of oligomers detected from integrating the fitted FRET efficiency peaks. For the sample collected after 14 hours of aggregation, there is a noticeable increase in the number of detected events as the ionic

strength of the dilution buffer is increased, suggesting that there are destabilizing charge repulsions in the earlier formed oligomers. Moreover, the destabilization (likely involving disaggregation) of the type A oligomers upon dilution into low ionic strength buffer conditions is rapid and occurs during the time it takes for the sample to be added to the instrument, since the same number of oligomeric events and FRET histograms are found when the sample is analyzed at later times. For the sample taken after 38 hours of aggregation, however, there is no significant effect of the ionic strength on the detected oligomers. The more compact, higher FRET efficiency oligomers are less susceptible to changes in ionic strength, than the earlier formed oligomers, which appear to be destabilized by charge repulsion. In addition to shielding the charge interactions, the higher ionic strength can also increase the stabilizing hydrophobic interactions, which could also account for the oligomers dissociating at lower salt concentrations.

Lowering the pH of the solution[21], increasing the salt concentration[25], or removing the C-terminal region of the protein has been demonstrated to drastically increase the rate of αS aggregation. Hoyer et al.[26], and Dedmon et al.[27] have suggested that the C-terminus interacts with the N-terminus in the monomeric form of the protein, shielding the NAC region, and preventing its self-assembly. At high ionic strengths, this interaction will be diminished, leading to an increased association of the monomers. However, the findings here suggest that it is not only the monomer conformation that is affected by varying the ionic strength of the solution, but the stability of the early-formed oligomers is also affected. At low ionic strengths, fewer early oligomers will be formed and therefore a decrease in the aggregation rate of the protein is expected as a consequence of a significant destabilization of these oligomers under those conditions.

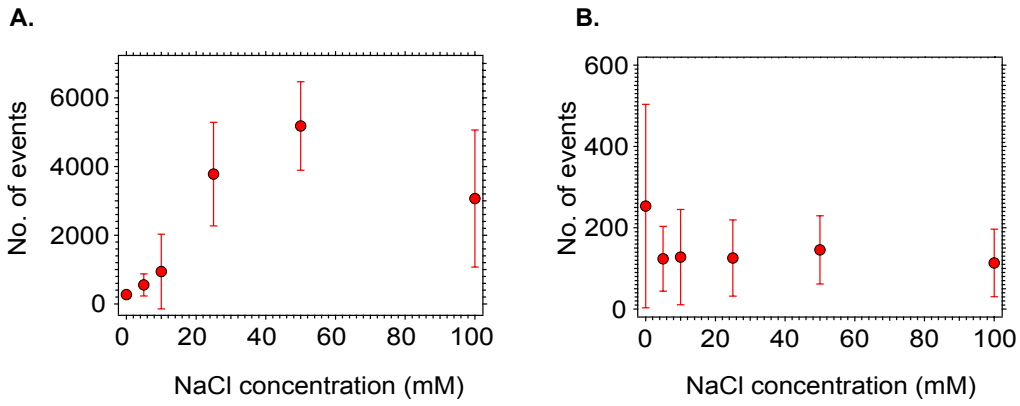

Figure 7. The effect of ionic strength on the number of events detected for aggregating samples of αS after 14 hours (A.) and 38 hours (B.) of aggregation (mean ± S.D., n = 3). The aggregation was done in 150 mM tris buffer with 100 mM NaCl, before being diluted into varying concentrations of NaCl. After 14 hours, there is a significant increase in the number of events detected with increasing sodium chloride concentration. After 38 hours, the effect of the varying ionic strength on the number of oligomers detected is not pronounced.

In a second series of experiments, αS was incubated in 25 mM Tris buffer with 100 mM NaCl under conditions favoring protein aggregation, and regular time-points were diluted into either 25 mM Tris with 100 mM NaCl, or into distilled water (pH 7) before being analyzed. *Figure 8A* shows the resulting 2D contour plots of size and FRET efficiency, FRET efficiency histograms are presented in *Figure 8B*, and the numbers of oligomers for each time-point when diluted into either Tris buffer, or distilled water are shown in *Figure 9*. The lower FRET efficiency oligomers (type A) were found to almost entirely dissociate on dilution into distilled water, whereas the high FRET efficiency oligomers (type B) are stable to dilution into distilled water, and do not dissociate.

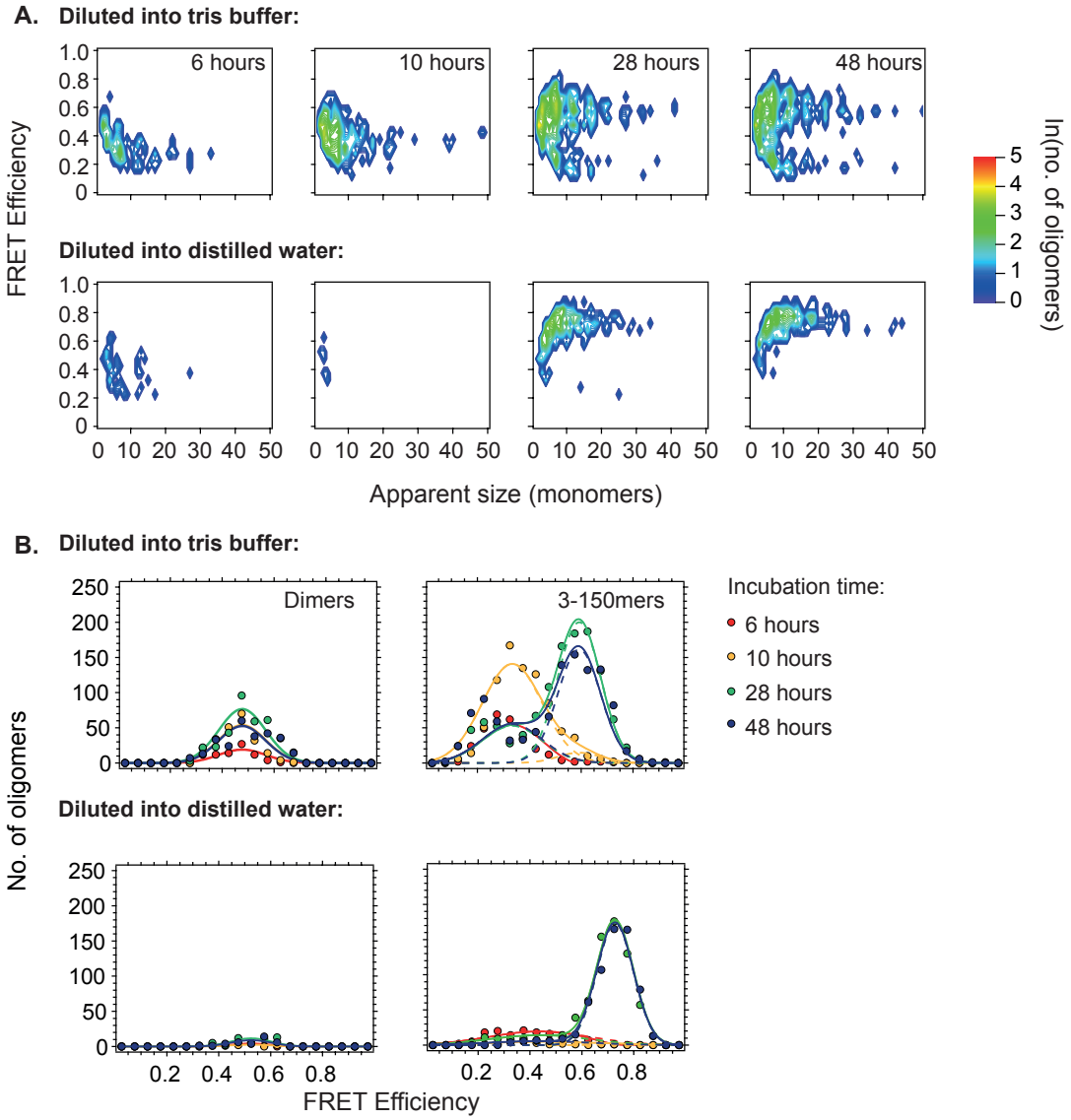

Figure 8. A. Representative 2D contour plots of size and FRET efficiency showing the effect of diluting the samples from an aggregating sample of αS into either 25 mM tris buffer with 100 mM NaCl or into distilled water. B. Representative FRET efficiency histograms of dimers and larger oligomers generated when the samples were either diluted into either 25 mM tris buffer with 100 mM NaCl or distilled water.

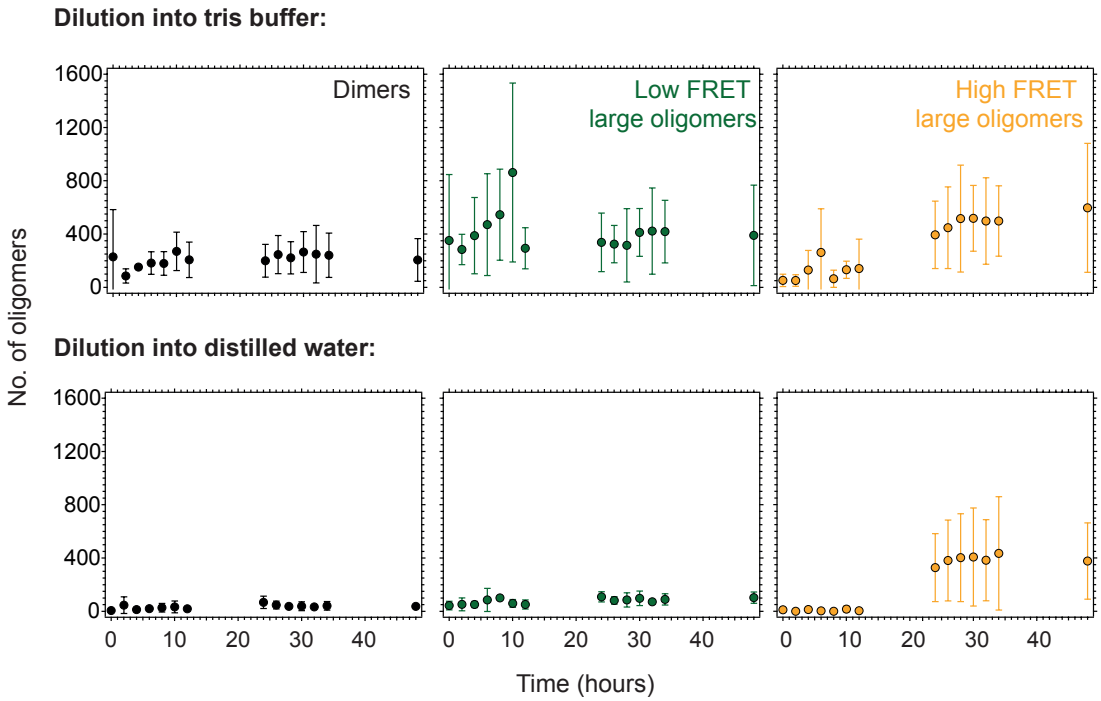

Figure 9 Kinetic traces of the different types of oligomer diluted either into 25 mM Tris buffer with 100 mM NaCl, or into distilled water (mean ± S.D., n = 3). The low FRET efficiency oligomers can be seen to be highly destabilized in low ionic strength solutions.

By diluting the samples into distilled water, it is therefore possible to separate the high FRET efficiency oligomers from the lower FRET efficiency ones. These are the oligomers that were previously identified as being the cytotoxic species[16], and this method highlights their greater stability, and allows them to be distinguished from the second population not only from their FRET efficiency, but also from their sensitivity to ionic strength.

SUMMARY

Through the use of a microfluidic device and fast-flow, it is possible to collect single-molecule data 150 times faster than using stationary measurements. At the shorter time accessible by this approach, two different populations of oligomers are observed during

the aggregation, one exhibiting a lower FRET efficiency, and one resulting from the conversion of these into more compact oligomers having a higher FRET efficiency. The data generated using this method has been further analyzed by fitting it to a simple kinetic model in which type A oligomers are first formed before being converted to type B oligomers, both of which can grow in size via monomer addition. The kinetic parameters determined from this fitting are analogous to those previously determined. Overall, the developments have reduced the time required to analyze a dataset from three hours to just over five minutes, allowing for greater time resolution, and also several experiments to be run simultaneously on one instrument, since numerous samples can be measured back-to-back within a short period of time.

The reduced time allows for further biophysical measurements to be made, and we have shown that by diluting the oligomeric samples into distilled water, the earlier formed lower FRET efficiency oligomers dissociate, possibly because of charge repulsions destabilizing the oligomers being less shielded. This finding allows for the isolation of the higher FRET efficiency, cytotoxic oligomeric species from a solution of oligomers, simply by changing the ionic strength of the buffer. Our findings substantiate the finding that there are two forms of oligomeric species generated when αS aggregates; not only do they differ in FRET efficiency and susceptibility to proteinase-K digestion, but they also behave differently when diluted into low ionic strength buffers.

Acknowledgements

M.H.H. and L.T. contributed equally to this work. M.H.H. thanks the Royal Society of Chemistry (Analytical Chemistry Trust Fund) for his studentship. L.T. has been the recipient of a grant PAT Post Doc Outgoing 2009 – 7th Framework Program Marie Curie COFUND actions. A.J.D. is funded by the Schiff Foundation.

Supporting Information Available. Justification for choice of dyes, the measurement parameters, details regarding the data analysis and modeling, and individual oligomer FRET histograms at different ionic strengths are included here. This material is available free of charge via the internet at http://pubs.acs.org

References

(1) Bertram, L.; Tanzi, R. E. *J. Clin. Invest.* **2005**, *115* (6), 1449–1457.
(2) Samii, A.; Nutt, J. G.; Ransom, B. R. *Lancet* **2004**, *363* (9423), 1783–1793.
(3) Jankovic, J. *J. Neurol. Neurosurg. Psychiatry* **2008**, *79* (4), 368–376.
(4) Spillantini, M. G.; Schmidt, M. L.; Lee, V. M.; Trojanowski, J. Q.; Jakes, R.; Goedert, M. *Nature* **1997**, *388* (6645), 839–840.
(5) Noe, E.; Marder, K.; Bell, K. L.; Jacobs, D. M.; Manly, J. J.; Stern, Y. *Mov. Disord. Off. J. Mov. Disord. Soc.* **2004**, *19* (1), 60–67.
(6) Lippa, C. F.; Schmidt, M. L.; Lee, V. M.; Trojanowski, J. Q. *Ann. Neurol.* **1999**, *45* (3), 353–357.
(7) Ahn, T.-B.; Kim, S. Y.; Kim, J. Y.; Park, S.-S.; Lee, D. S.; Min, H. J.; Kim, Y. K.; Kim, S. E.; Kim, J.-M.; Kim, H.-J.; Cho, J.; Jeon, B. S. *Neurology* **2008**, *70* (1), 43–49.
(8) Singleton, A. B.; Farrer, M.; Johnson, J.; Singleton, A.; Hague, S.; Kachergus, J.; Hulihan, M.; Peuralinna, T.; Dutra, A.; Nussbaum, R.; Lincoln, S.; Crawley, A.; Hanson, M.; Maraganore, D.; Adler, C.; Cookson, M. R.; Muenter, M.; Baptista, M.; Miller, D.; Blancato, J.; Hardy, J.; Gwinn-Hardy, K. *Science* **2003**, *302* (5646), 841.
(9) Polymeropoulos, M. H.; Lavedan, C.; Leroy, E.; Ide, S. E.; Dehejia, A.; Dutra, A.; Pike, B.; Root, H.; Rubenstein, J.; Boyer, R.; Stenroos, E. S.; Chandrasekharappa, S.; Athanassiadou, A.; Papapetropoulos, T.; Johnson, W. G.; Lazzarini, A. M.; Duvoisin, R. C.; Di Iorio, G.; Golbe, L. I.; Nussbaum, R. L. *Science* **1997**, *276* (5321), 2045–2047.
(10) Krüger, R.; Kuhn, W.; Müller, T.; Woitalla, D.; Graeber, M.; Kösel, S.; Przuntek, H.; Epplen, J. T.; Schöls, L.; Riess, O. *Nat. Genet.* **1998**, *18* (2), 106–108.
(11) Zarranz, J. J.; Alegre, J.; Gómez-Esteban, J. C.; Lezcano, E.; Ros, R.; Ampuero, I.; Vidal, L.; Hoenicka, J.; Rodriguez, O.; Atarés, B.; Llorens, V.; Gomez Tortosa, E.; del Ser, T.; Muñoz, D. G.; de Yebenes, J. G. *Ann. Neurol.* **2004**, *55* (2), 164–173.
(12) Ghosh, D.; Mondal, M.; Mohite, G. M.; Singh, P. K.; Ranjan, P.; Anoop, A.; Ghosh, S.; Jha, N. N.; Kumar, A.; Maji, S. K. *Biochemistry (Mosc.)* **2013**, *52* (40), 6925–6927.
(13) Lesage, S.; Anheim, M.; Letournel, F.; Bousset, L.; Honoré, A.; Rozas, N.; Pieri, L.; Madiona, K.; Dürr, A.; Melki, R.; Verny, C.; Brice, A.; French Parkinson's Disease Genetics Study Group. *Ann. Neurol.* **2013**, *73* (4), 459–471.
(14) Conway, K. A.; Harper, J. D.; Lansbury, P. T. *Biochemistry (Mosc.)* **2000**, *39* (10), 2552–2563.
(15) Winner, B.; Jappelli, R.; Maji, S. K.; Desplats, P. A.; Boyer, L.; Aigner, S.; Hetzer, C.; Loher, T.; Vilar, M.; Campioni, S.; Tzitzilonis, C.; Soragni, A.; Jessberger, S.; Mira, H.; Consiglio, A.; Pham, E.; Masliah, E.; Gage, F. H.; Riek, R. *Proc. Natl. Acad. Sci. U. S. A.* **2011**, *108* (10), 4194–4199.
(16) Cremades, N.; Cohen, S. I. A.; Deas, E.; Abramov, A. Y.; Chen, A. Y.; Orte, A.; Sandal, M.; Clarke, R. W.; Dunne, P.; Aprile, F. A.; Bertoncini, C. W.; Wood, N. W.; Knowles, T. P. J.; Dobson, C. M.; Klenerman, D. *Cell* **2012**, *149* (5), 1048–1059.
(17) Outeiro, T. F.; Putcha, P.; Tetzlaff, J. E.; Spoelgen, R.; Koker, M.; Carvalho, F.; Hyman, B. T.; McLean, P. J. *PloS One* **2008**, *3* (4), e1867.

(18) Orte, A.; Birkett, N. R.; Clarke, R. W.; Devlin, G. L.; Dobson, C. M.; Klenerman, D. *Proc. Natl. Acad. Sci. U. S. A.* **2008**, *105* (38), 14424–14429.
(19) Narayan, P.; Meehan, S.; Carver, J. A.; Wilson, M. R.; Dobson, C. M.; Klenerman, D. *Biochemistry (Mosc.)* **2012**, *51* (46), 9270–9276.
(20) Narayan, P.; Holmström, K. M.; Kim, D.-H.; Whitcomb, D. J.; Wilson, M. R.; St. George-Hyslop, P.; Wood, N. W.; Dobson, C. M.; Cho, K.; Abramov, A. Y.; Klenerman, D. *Biochemistry (Mosc.)* **2014**, *53* (15), 2442–2453.
(21) Uversky, V. N.; Li, J.; Fink, A. L. *J. Biol. Chem.* **2001**, *276* (14), 10737–10744.
(22) Uversky, V. N.; Li, J.; Fink, A. L. *J. Biol. Chem.* **2001**, *276* (47), 44284–44296.
(23) Horrocks, M. H.; Li, H.; Shim, J.-U.; Ranasinghe, R. T.; Clarke, R. W.; Huck, W. T. S.; Abell, C.; Klenerman, D. *Anal. Chem.* **2012**, *84* (1), 179–185.
(24) Clarke, R. W.; Orte, A.; Klenerman, D. *Anal. Chem.* **2007**, *79* (7), 2771–2777.
(25) Munishkina, L. A.; Henriques, J.; Uversky, V. N.; Fink, A. L. *Biochemistry (Mosc.)* **2004**, *43* (11), 3289–3300.
(26) Hoyer, W.; Antony, T.; Cherny, D.; Heim, G.; Jovin, T. M.; Subramaniam, V. *J. Mol. Biol.* **2002**, *322* (2), 383–393.
(27) Dedmon, M. M.; Lindorff-Larsen, K.; Christodoulou, J.; Vendruscolo, M.; Dobson, C. M. *J. Am. Chem. Soc.* **2005**, *127* (2), 476–477.

MATERIALS AND METHODS

Protein expression and purification. BL21(DE3) Gold cells (Stratagene) were transformed with the Cys mutant A90C. Starters were diluted into Overnight Express™ Instant TB Medium (Novagen) supplemented with 1% glycerol and left to grow for 16-18 h at 30°C. Following this, cells were harvested and the protein purified as previously published[16].

Device fabrication. Microfluidic channels were fabricated using standard soft-lithography techniques into polydimethylsiloxane (PDMS; Dow Corning) with SU-8 photoresist on silicon masters, as described previously[23]. The channels were plasma-bonded to glass coverslides (V.W.R., thickness = 1) to create sealed devices. The channel height was 25 μm. Each device was inspected on a white-light microscope (Nikon Ti-U), and only those without dust or aberrations were used.

Protein labeling. The Cys variant of wild-type αS was labeled as reported previously[16]. Life Technologies Alexa Fluor 488 C_5 maleimide (AF488) and Alexa Fluor 594 C_5 maleimide (AF594) were used in these reactions. Labeled protein was isolated from unreacted dye using the method reported in Cremades et al., 2012[16]. The reaction yield was checked by mass spectrometry for all reactions, and all labeling reactions with a yield lower than 90% were discarded.

Single-molecule fluorescence measurements of aggregating αS. A 70 μM solution made up of equimolar concentrations of AF488 and AF594 labeled αS was prepared in 25 mM Tris-HCl, pH 7.4, 100 mM NaCl. The buffer was freshly prepared before each experiment, and passed through a 0.02 μm syringe filter (Anotop, Whatman) to remove insoluble contaminants. The aggregation mixture was supplemented with 0.01% NaN_3 to

prevent bacterial growth, and was then incubated at 37°C with orbital shaking at 200 r.p.m. (25 mm orbital diameter). Regular time-points were taken throughout the course of the aggregation and were immediately diluted by a factor of 1:250,000 (in two stages) before being loaded into a 200 μL gel-loading tip (Life technologies, Carlsbad, CA, USA) attached to the inlet port of a microfluidic channel (25 μm in height, 100 μm in width, 1 cm in length) mounted onto the single-molecule confocal microscope. The confocal volume was focused 10 μm into the center of the channel, and the solution was passed through the channel at an average velocity of 2 cm/s by applying a negative pressure, which was generated using a syringe pump (Harvard apparatus, Holliston, MA, USA) attached to the outlet port via Fine Bore Polyethylene Tubing (0.38 mm inner-diameter, 1.09 mm outer-diameter; Smiths Medical International, Hythe, Kent, UK). Before adding the gel-loading tip, and withdrawing the sample, the syringe, tubing and microfluidic channel were first filled with buffer and any air-bubbles were purged from the system. After the appearance of single-molecule bursts corresponding to labeled αs passing through the confocal volume, the sample was measured for 400 s. There was no noticeable decrease in the event-rate over the duration of the measurement, suggesting that any surface absorbance does not affect the measurement.

Single-molecule instrumentation. A Gaussian laser beam at a wavelength of 488 nm was first attenuated using neutral density filters, and passed through a spatial filter to before being directed through the back-port of an inverted microscope (Nikon Ti-U). A dichroic mirror (Di01-R405/488/594 Semrock) reflected the laser light through an oil-immersion objective (Nikon CFI Plan Apochromat VC 60X Oil N2 NA 1.4, W.D 0.13 mm), which focuses it to a diffraction-limited confocal spot within the sample being

studied. The emitted fluorescence was collected by the same objective and passed through the dichroic, before being focused by a tube lens within the microscope body through a 50 μm pinhole (Thorlabs). A second dichroic (585DRLP Horiba) then separates the fluorescence from the two different fluorophores; the longer wavelength passes through the dichroic and was focused by a lens (Plano apo convex, focal length = 50 mm, Thorlabs) through a band pass filter (FF01-629/53) onto the Avalanche Photodiode (APD) detector. The shorter wavelength was reflected by the dichroic and is focused through a second set of filters (535AF55 Horiba, 540LP Omega) onto the second APD. Outputs from the two APDs are connected to a custom-programmed field-programmable gate array, FPGA (Colexica), which counts the signals and combines them into time-bins, which are selected according to the expected residence time of molecules traveling through the confocal volume.

Stability in different ionic strength solutions. To determine the stability of different samples of αS oligomers with respect to varying ionic strength, the solution of αS was diluted by a factor of 1:250,000 into a 5 mM tris buffer (pH 7.4) containing a range of NaCl concentrations (from 0 to 100 mM). The diluted sample was then immediately analyzed on the single-molecule confocal instrument.